The free-fall time of finite sheets and filaments

Jesús A. Toalá, Enrique Vázquez-Semadeni & Gilberto C. Gómez

Centro de Radioastronomía y Astrofísica, Universidad Nacional Autónoma de México,

Campus Morelia

Apartado Postal 3-72, 58090, Morelia, Michoacán, México

To appear in The Astrophysical Journal

Received _____; accepted _____

ABSTRACT

Molecular clouds often exhibit filamentary or sheet-like shapes. We compute the free-fall time ($\tau_{\rm ff}$) for finite, uniform, self-gravitating circular sheets and filamentary clouds of small but finite thickness, so that their volume density ρ can still be defined. We find that, for thin sheets, the free-fall time is larger than that of a uniform sphere with the same volume density by a factor proportional to $\sqrt{A}$, where the aspect ratio A is given by $A = R/h$, R being the sheet's radius and h is its thickness. For filamentary clouds, the aspect ratio is defined as $A = L/\mathcal{R}$, where L is the filament's half length and $\mathcal{R}$ is its (small) radius, and the modification factor is a more complicated, although in the limit of large A it again reduces to nearly $\sqrt{A}$. We propose that our result for filamentary shapes naturally explains the ubiquitous configuration of clumps fed by filaments observed in the densest structures of molecular clouds. Also, the longer free-fall times for non-spherical geometries in general may contribute towards partially alleviating the "star-formation conundrum", namely, that the star formation rate in the Galaxy appears to be proceeding in a timescale much larger than the total molecular mass in the Galaxy divided by its typical free-fall time. If molecular clouds are in general formed by thin sheets and long filaments, then their relevant free-fall time may have been systematically underestimated, possibly by factors of up to one order of magnitude.

Subject headings: ISM: clouds — ISM: structure

1. Introduction

The so-called free-fall time is one of the most important quantities in astrophysics. For a spherical object of mass M and radius R, this timescale is given by (see, e.g., Binney & Tremaine 1987)

$$\tau_{\rm ff} \equiv \sqrt{\frac{\pi^2 R^3}{8GM}} = \sqrt{\frac{3\pi}{32G\rho}}; \tag{1}$$

where in the second equality we have introduced the volume density defined by

$$\rho(M,R) = \frac{3M}{4\pi R^3}. \tag{2}$$

The timescale $\tau_{\rm ff}$ has the interesting property that it depends on the object's size and mass only through a combination that is proportional to its volume density, ρ. That is, once ρ is specified, $\tau_{\rm ff}$ is independent of the object's mass (or size), implying that, in a collapsing uniform-density sphere, all spherical shells reach the center at the same time. This is equivalent to the well-known property that, for spherically-symmetric perturbations of a uniform medium, the growth rate increases with increasing wavelength, and thus the fastest mode of collapse is an overall contraction of the medium (Tohline 1980; Larson 1985).

However, this independence of $\tau_{\rm ff}$ from the actual physical dimensions of an object of fixed volume density is only valid when the object's extension R is comparable in all three spatial dimensions (a "3D object"), because only in this case is the volume density of the object given by eq. (2). Instead, for nearly sheet-like ("2D") or filamentary ("1D") shapes, the volume density ρ is *not* proportional M/L^3, where L here generically denotes the object's largest dimension. For these morphologies, $\rho \propto M/(\ell L^2)$ or $\rho M/(L\ell^2)$, respectively, where ℓ denotes the fixed, small dimension(s) of the object. This is relevant for interstellar structures, since they are often observed to have sheet-like or filamentary, rather than spherical, morphologies (e.g. Bally et al. 1989; de Geus et al. 1990; Heiles & Troland 2003;

Myers 2009; Molinari et al. 2010; André et al. 2010). This suggests that the free-fall timescale may actually depend on the size of a non-spherical object in addition to depending its volume density.

The gravitational stability of non-spherical structures has been considered in earlier works (e.g., Ledoux 1951; Larson 1985; Curry 2000), but mostly considering *infinite* media and without discussing collapse timescales. Finite-size non-spherical structures, and their corresponding collapse times have only recently begun to be considered. In particular, Burkert & Hartmann (2004) computed an approximation to the free-fall time $\tau_{\rm ff,2D}$ for finite-sized, infinitely thin circular sheets of radius R, given by

$$\tau_{\rm ff,2D} \approx \tau_{\rm ff,BH} \equiv \sqrt{\frac{R}{\pi G \Sigma}}, \tag{3}$$

where Σ is the surface density (with units of mass per unit area) of the sheet. It is noteworthy that, in this case, the free-fall time exhibits a dependence on its size in addition to depending on the (column) density. Indeed, numerical simulations of the collapse of large sheet-like clouds containing many Jeans masses by Vázquez-Semadeni et al. (2007) exhibited collapse timescales significantly larger than their corresponding three-dimensional free-fall time, as given by eq. (1). Motivated by these realizations, in this paper we compute in detail the free-fall time for sheet-like and filamentary structures. Note that Pon et al. (2011) have recently investigated the free-fall timescales for sheet-like and filamentary geometries, although they have focused on whether small-scale perturbations within such structures have sufficient time to collapse before the whole structure does so. Here we concentrate on a different question: whether the collapse timescale for these geometries is longer, and by what amount, compared to their spherical counterparts. Thus, our study and that by Pon et al. (2011) can be considered as being complementary to each other.

2. The spherical case

The standard calculation of the free-fall time for a uniform-density sphere proceeds as follows (e.g., Binney & Tremaine 1987). Consider a uniform sphere of radius R, mass M, and volume density $\rho = \rho_{\rm 3D}(M,R) \equiv 3M/4\pi R^3$, which at time $t = 0$ starts to contract under the action of its self-gravity exclusively. The subindex "3D" denotes the *function* that is used to calculate a quantity for a spherical (or "3D") geometry, which we distinguish from the *physical value* of the quantity itself, denoted without subscript. At a certain later time $t > 0$, when the sphere has radius $r < R$, the velocity of a point at its periphery is

$$\frac{dr}{dt} = -\sqrt{2GM\left(\frac{1}{r} - \frac{1}{R}\right)}. \tag{4}$$

Introducing the non-dimensional variable $x \equiv r/R$, this is equivalent to

$$\frac{dx}{dt} = -\sqrt{\frac{2GM}{R^3}\left(\frac{1-x}{x}\right)}. \tag{5}$$

It is then clear that, because for a spherically symmetric uniform object the mass M increases as R^3, expression (5) depends on the mass and size of the sphere only through the volume density they imply, $\rho = \rho_{\rm 3D}$. Equation (5) can then be integrated to yield

$$\tau_{\rm ff} = \tau_{\rm ff,3D}(M,R) = \left(\frac{R^3}{2GM}\right)^{1/2} \int_0^1 \left(\frac{x}{1-x}\right)^{1/2} dx = \sqrt{\frac{3\pi}{32G\rho}}, \tag{6}$$

evidencing the independence of $\tau_{\rm ff}$ on the cloud's size or mass for a given volume density.

3. Circular sheet-like cloud

Let us now consider the case of an infinitely thin circular sheet of mass M, initial radius R, and uniform surface density $\Sigma = M/\pi R^2$. Here we follow closely the analysis by Burkert & Hartmann (2004, hereafter BH04). They calculated the radial acceleration experienced by the periphery of the sheet when it has shrunk to radius $r < R$, under

the assumption that the surface density Σ remains constant. This assumption was made because they found that the maximum acceleration occurs at the periphery of the sheet, and thus a dense contracting ring forms in the periphery, while the inner surface density remains essentially unchanged. This behavior has been observed in numerical simulations by BH04 themselves and by Vázquez-Semadeni et al. (2007). With this assumption, BH04 found

$$a_r = 4G\Sigma\frac{R}{r}\left[K\left(\frac{r}{R}\right) - E\left(\frac{r}{R}\right)\right], \tag{7}$$

where K and E are respectively the first and second elliptic integrals. Upon a series expansion, eq. (7) becomes

$$a_r = \pi G\Sigma\left[\frac{r}{R} + \frac{3}{8}\left(\frac{r}{R}\right)^3 + \frac{45}{192}\left(\frac{r}{R}\right)^5 + \cdots\right]. \tag{8}$$

Note that the acceleration diverges at $r = R$, but BH04 noted that this problem is eliminated when a finite sheet thickness is considered.

BH04 retained only the linear term in eq. (8) and computed the free-fall time by noting that $a_r = dv/dt = 1/2\ dv^2/v\ dt = 1/2\ dv^2/dr$, where v is the instantaneous radial velocity. They thus found the instantaneous velocity as a function of the instantaneous radius of the sheet, given by

$$v^2(r) = -\frac{2\pi G\Sigma}{R}\int_R^r r'dr' = \frac{\pi G\Sigma}{R}\left(R^2 - r^2\right), \tag{9}$$

implying that the radial velocity at the end of the collapse is

$$v(r = 0) = \sqrt{\pi G\Sigma R}. \tag{10}$$

Taking this as a representative velocity for the entire collapse, BH04 then found a lower limit to the time for the sheet to shrink from $r = R$ to $r = 0$, which we label $\tau_{\rm ff,BH}$, given by

$$\tau_{\rm ff,BH} = \frac{R}{v(r = 0)} = \sqrt{\frac{R}{\pi G\Sigma}}, \tag{11}$$

as anticipated in eq. (3).

At this point we can extend the calculations by BH04 in two ways. First, we consider clouds with small but finite thickness, so that it is possible to define a *volume* density within them. We refer to this as a "quasi-2D" geometry. Specifically, we rewrite the surface density assuming a small but finite thickness h such that $\Sigma = \rho h$, where ρ is the volume density. However, in this case the volume density is not given by eq. (2), but rather by $\rho = \rho_{\rm 2D}(M, R) = M/\pi R^2 h$. Here, the subindex "2D" now denotes the relevant function to compute the quantity for a quasi-2D structure.

Second, instead of taking the final velocity as representative of the entire collapse, we can obtain a more accurate expression by integrating eq. (8) from R to r to write an expresion for $v(r)$, obtaining

$$v_1(r) = \sqrt{\frac{\pi G \rho}{A}\,(R^2 - r^2)}, \tag{12}$$

where $A \equiv R/h$ is the *aspect ratio*. After a second integration we obtain

$$r_1(t) = R\ \sin\left(\frac{\pi}{2} - \sqrt{\frac{\pi G \rho}{A}}t\right), \tag{13}$$

where the subindex '1' denotes the assumption that the density of the sheet internal to its periphery remains constant. Setting $r_1 = 0$, we obtain the corresponding free fall time as

$$\tau_{\rm ff,1} = \sqrt{\frac{A\pi}{4G\rho}} = \sqrt{\frac{8A}{3}}\tau_{\rm ff,3D}, \tag{14}$$

where the second equality compares with the free-fall time that would be obtained for a spherical structure with the same volume density, explicitly exhibiting the extra factor $\propto \sqrt{A}$.

Let us now assume that, instead of remaining constant, the sheet's density increases during the contraction so as to maintain the sheet's mass constant; that is, $\Sigma\left(r(t)\right) = M/\pi r(t)^2 = \rho\left(r(t)\right) h$, with $M = $ cst. Note that, in reality, the sheet's mass

does remain constant during the collapse, but it is not distributed uniformly on the sheet. Instead, the mass external to r is piled up at the periphery. So, a point at the periphery sees this mass at the farthest possible distance within the sheet, rather than seeing it uniformly distributed over the sheet. Thus, the constant-mass assumption overestimates the gravitational pull of the sheet on this point. On the other hand, the constant-density assumption neglects the mass at the periphery altogether. Thus, the two assumptions should bracket the real situation (still within the linear approximation).

Under this assuption we can integrate eq. (8) from R to r to obtain a velocity function as

$$v_2(r) = \sqrt{2\pi G\rho h R \ln\left(\frac{R}{r}\right)} = \sqrt{\frac{2\pi G\rho R^2}{A}\ln\left(\frac{R}{r}\right)}, \tag{15}$$

where the subindex '2' denotes the case of a constant-mass assumption. Upon a second integration, we obtain

$$r_2(t) = \frac{R}{\exp\left[\mathrm{erf}^{-1}\left(\sqrt{\frac{2G\rho}{A}}t\right)\right]^2}, \tag{16}$$

where erf^{-1} is the inverse error function. This gives a free-fall time of

$$\tau_{\mathrm{ff},2} = \sqrt{\frac{A}{2G\rho}} = \sqrt{\frac{16A}{3\pi}}\tau_{\mathrm{ff,3D}}, \tag{17}$$

which is $\sim 25\%$ shorter than $\tau_{\mathrm{ff},1}$ because the gravitational acceleration is always larger, as the surface density increases monotonically as the sheet contracts. The estimates for the free-fall time in the two cases differ by factors of order unity at most. More importantly, both of them have the same dependence on the aspect ratio as $\sim\sqrt{A}$. This dependence is fundamentally different from that of the spherical ("3D") case, given by eq. (6), as discussed in Sec. 1. This is illustrated in Fig.1 (*Top panels*), which shows the infall velocities as a function of the instantaneous radius, corresponding to eqs. (12) and (15), taking $R = \rho = G = 1$, for a range of values of A. Also shown is the infall velocity for the spherical case. We see that the latter is always larger than either A values in both cases. This result

is clearly a consequence of the much smaller mass contained in a flat, essentially "2D", configuration than in a spherical (3D) one of the same volume density.

The *bottom panels* of Fig. 1 show the sheet's radius as a function of time for the two density cases. As expected, case 1, in which the cloud's mass is not conserved, but rather decreases in time, undergoes a slightly slower collapse than case 2. Nevertheless, we see that the difference in the collapse time between the two cases is around $\sim 25\%$, and so both are qualitatively similar.

4. Filamentary cloud

We now consider the case of a uniform, cylindrical cloud of total length $2L$, radius $\mathcal{R} \ll L$, and volume density $\rho = \rho_{\rm 1D}(M, L) = M/\pi\mathcal{R}^2 L$, where now the subindex '1D' denotes the function appropriate for calculating a physical quantity in the quasi-1D case. Note that here the filament's radius $\mathcal{R}$ is the small, fixed dimension, and the size variable is L.

Again, we start with the case in which the filament's density remains constant. In this case, the acceleration towards the filament's center at a distance l from the center is given by (BH04)

$$a(l) = \frac{1}{2}\frac{dv^2}{dl} = -2\pi G\rho\left[2l + \mathcal{R} - \sqrt{\mathcal{R}^2 + 4l^2}\right]. \tag{18}$$

Integrating this equation from L to l, we obtain the radial velocity after the filament has contracted from L to l:

$$v(l) = \sqrt{4\pi G\rho}\left[(L-l)(L+l+\mathcal{R}) - \frac{L}{2}\sqrt{\mathcal{R}^2+4L^2} + \frac{l}{2}\sqrt{\mathcal{R}^2+4l^2} - \frac{\mathcal{R}^2}{4}\ln\left|\frac{\sqrt{\mathcal{R}^2+4L^2}+2L}{\sqrt{\mathcal{R}^2+4l^2}+2l}\right|\right]^{1/2}. \tag{19}$$

If we now define the nondimensional parameters $A = L/\mathcal{R}$ and $x = l/L$, we can rewrite eq.

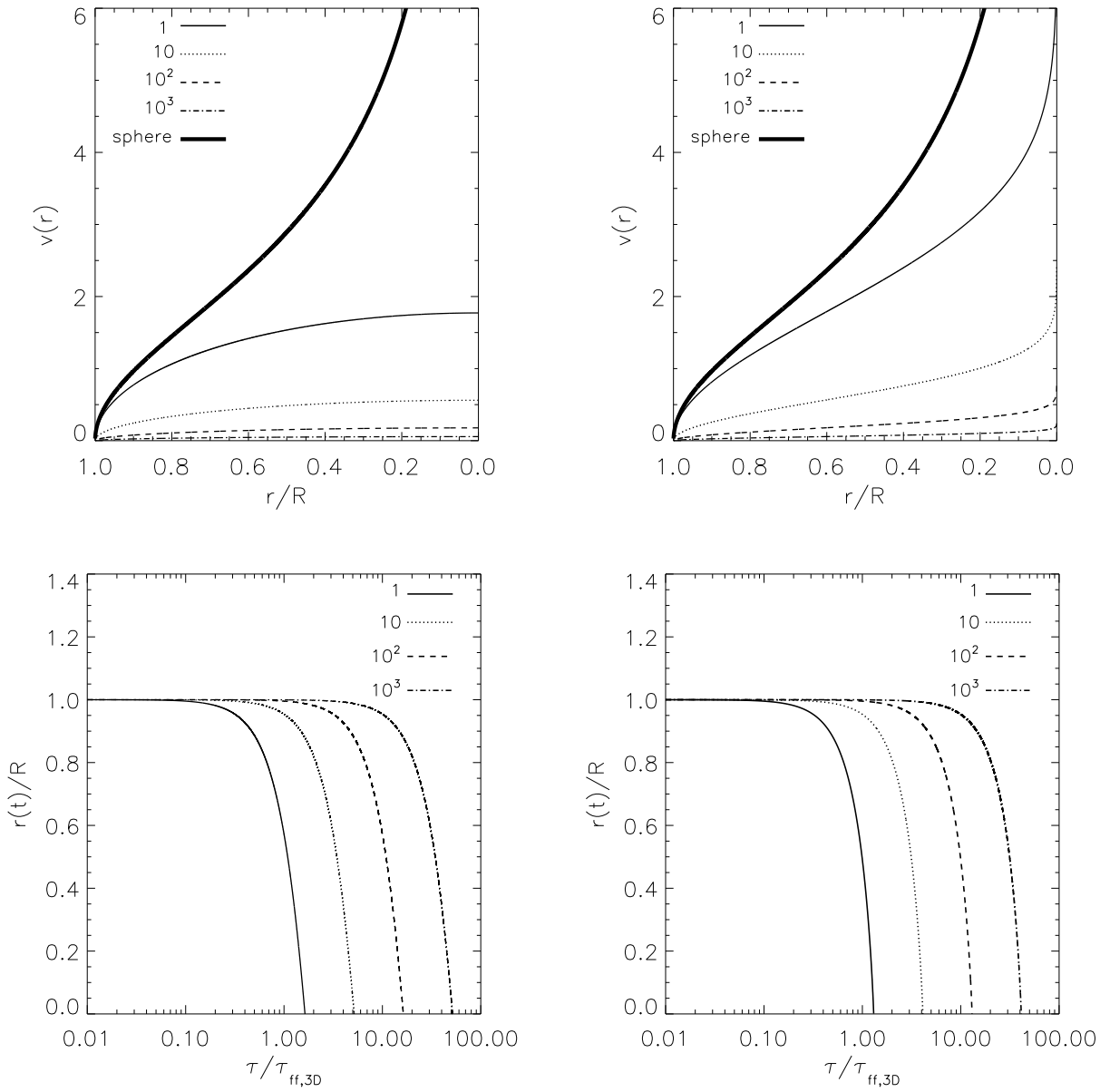

Fig. 1.— *Top:* Evolution of the radial velocity of a sheet's periphery (shown as a function of its instantaneous radius, normalized to its initial value R) as it collapses, compared to the corresponding velocity for a spherical cloud (thick line). Note that the radius decreases to the right. *Bottom:* Normalized position of the sheet's radius as a function of time, in units of the spherical free-fall time. *Left:* Case 1. *Right:* Case 2. The different lines show different values of A.

(19) as

$$\frac{dx}{dt} = \frac{\pi}{2\tau_{\rm ff,3D}}\sqrt{\frac{3}{2}}\left[(1-x)(1+x+\frac{1}{A}) - \frac{1}{2}\sqrt{\frac{1}{A^2}+4} + \frac{x}{2}\sqrt{\frac{1}{A^2}+4x^2} - \frac{1}{4A^2}\ln\left|\frac{\sqrt{\frac{1}{A^2}+4}+2}{\sqrt{\frac{1}{A^2}+4x^2}+2x}\right|\right]^{1/2}. \tag{20}$$

This equation again shows that the velocity depends on the "aspect ratio" $A = L/\mathcal{R}$, besides the standard dependence on density given by $\tau_{\rm ff,3D}$.

Let us now drop the constant-density assumption and assume instead that the volume density increases as the filament contracts as $\rho(l) = \rho_{\rm 1D}(M, l) = M/\pi\mathcal{R}^2 l$. In this case, we can perform the same calculation for the velocity evolution, to obtain

$$\frac{dx}{dt} = \frac{\pi}{2\tau_{\rm ff,3D}}\sqrt{\frac{3}{2}}\left[2(1-x) - \sqrt{\frac{1}{A^2}+4} + \sqrt{\frac{1}{A^2}+4x^2} - \frac{1}{A}\ln\left|\frac{\sqrt{\frac{1}{A^2}+4x^2}+\frac{1}{A}}{\sqrt{\frac{1}{A^2}+4}+\frac{1}{A}}\right|\right]^{1/2}. \tag{21}$$

In Fig. 2 (*top panels*) we show the contraction velocity as a function of l for a range of values of A, for both the constant-density and constant-mass cases. In both, the final velocity reaches smaller values as larger values of A are considered. The *lower panels* in Fig. 2 show the position of the filament's edge as a function of time, obtained from numerical integration of eqs. (20) and (21). The results are normalized to the spherical free-fall time.

Expressions (20) and (21) are quite complicated, and thus it is worthwhile to consider the limiting case of large A, for which an analytical solution can be found. We obtain

$$\tau_{\rm ff,1} = \frac{2}{\pi}\sqrt{\frac{8A}{3}}\tau_{\rm ff,3D} \tag{22}$$

and

$$\tau_{\rm ff,2} = \sqrt{\frac{8A}{3\pi}}\tau_{\rm ff,3D}, \tag{23}$$

from which we see that, at large A, the free-fall time for filaments also exhibits an additional factor $\propto \sqrt{A}$ (Fig. 3), similarly to the case for sheets.

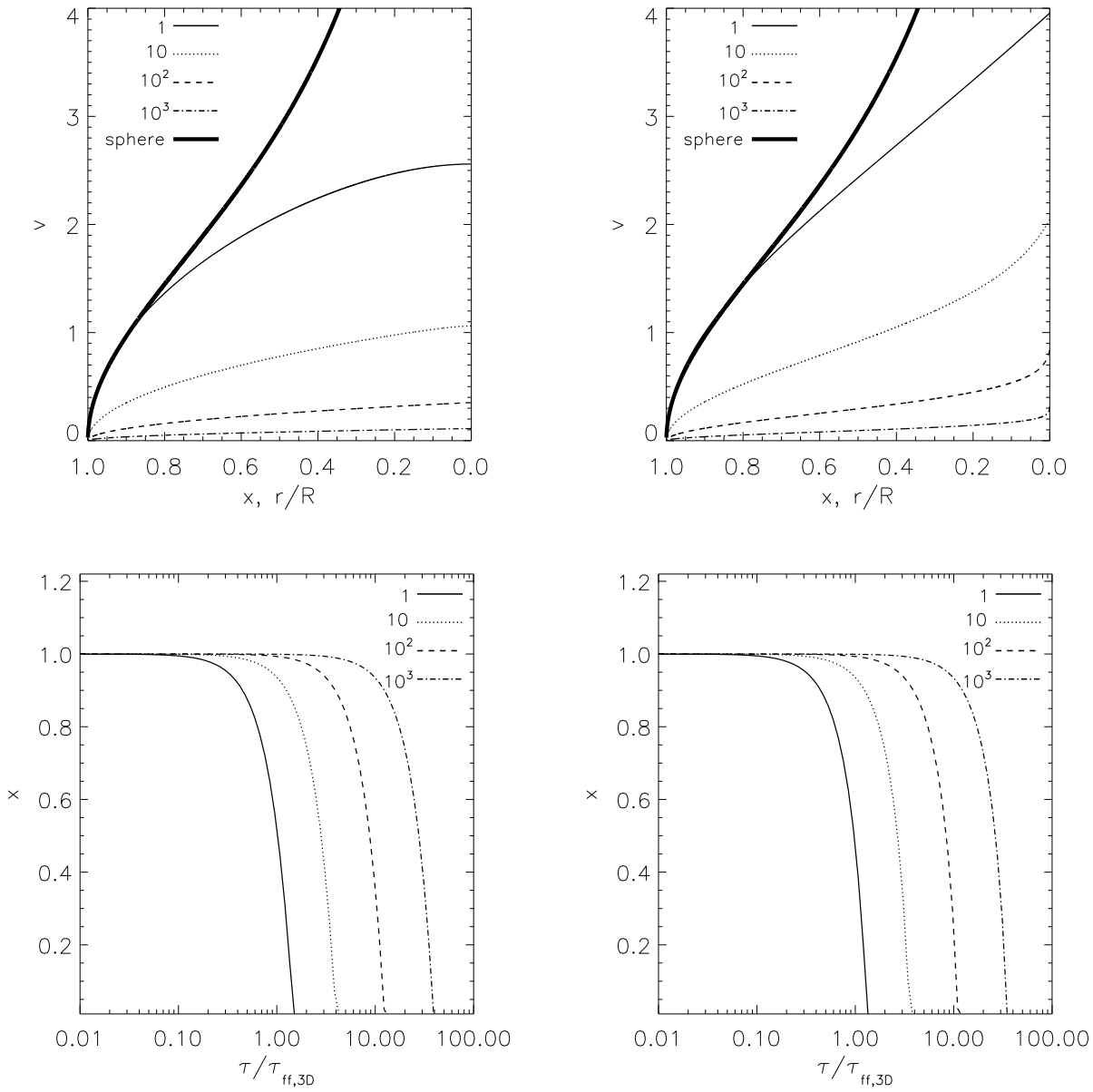

Fig. 2.— *Top:* Evolution of the edge velocity for a filamentary cloud, compared to the corresponding velocity for a spherical cloud (thick line). *Bottom:* Normalized position of the filament's edge as a function of time, normalized to the spherical free-fall time estimate. *Left:* Case 1, with $\rho = \text{cst}$. *Right:* Case 2, taking $\rho(l) = M/\pi\mathcal{R}^2 l$. The different lines show different values of A.

5. Discussion and applications

5.1. Implications for filamentary structure in molecular clouds

Our results have a number of implications for various aspects of interstellar structure and star formation. First, the fact that both the sheet-like and filamentary geometries have free-fall timescales larger than those of their three-dimensional (spherical) counterpart with the same volume density implies that any sheet or filament containing many Jeans masses will collapse *later* than any approximately-3D clump within it containing *one* Jeans mass. That is, the 3D clump will collapse on roughly one spherical free-fall time, while the sheet or filament around it will terminate its own collapse after a time that is longer by a factor $\sqrt{A}$. This naturally explains the commonly observed morphology of clumps immersed within, and accreting from, filaments (e.g. Myers 2009; Purcell et al. 2009; Schneider et al. 2010; Pillai et al. 2011), because the clumps evolve on a shorter timescale than their parent filaments.

Specifically, our results can be applied to the filaments observed in the Aquila rift and Polaris Flare regions by André et al. (2010). These authors report a typical filament width of $2\mathcal{R} \sim 10^4$ AU, or ~ 0.05 pc. In turn, filaments extending for over 3 pc can be readily seen in their Fig. 1, implying aspect ratios of up to ~ 60. From our Fig. 3, we see that this in turn implies filament collapse times up to ~ 10 times larger than the corresponding spherical one. Moreover, André et al. (2010) report a typical column density of the filaments of $N \sim 10^{22}$ cm^{-2}. We can thus estimate the mean volume density in the filaments as $n \approx N/2\mathcal{R} \approx 6.5 \times 10^4$ cm^{-3}, for which, assuming a mean molecular mass $\mu = 2.36$, the *spherical* free fall time is $\tau_{\rm ff,3D} \approx 1.3 \times 10^5$ yr, and the Jeans length is $L_{\rm J} \approx 0.08$ pc. According to our results, a filament of length $2L = 3$ pc would thus take a time ~ 1.3 Myr to collapse. But if it contracts towards its center of mass, then quickly the central parts of the filament will reach a volume density large enough that a segment of the

filament of length equal to its thickness will become Jeans unstable. Indeed, the required volume density for the Jeans length to become $L_{\rm J} = 2\mathcal{R} = 0.05$ pc is $n_{\rm J} \sim 1.8 \times 10^5$ cm^{-3}, or only ~ 2.8 times the mean volume density of the filament. At this point, the central clump becomes locally Jeans unstable, and proceeds to collapse on a timescale up to one order of magnitude shorter than the filament, naturally producing a star-forming core with a filamentary "appendix" that accretes onto it. Moreover, this will cause the core to sustain star formation for times significantly longer than its own (spherical) free-fall time, since its gas supply is continuously replenished by the accretion flow from the filament.

In turn, filaments may form from the collapse of sheets. As mentioned in sec. 3, during the collapse of a thin sheet, the acceleration is maximal at the edge, and thus the collapse occurs from the outside in, forming a dense ring in the periphery, which is topologically equivalent to a filament. Such hierarchical fragmentation from sheets to filaments has been suggested by several authors (Schneider & Elmegreen 1979; Gaida et al. 1984; Hanawa et al. 1993; Kofman & Pogosyan 1995), and has also been readily observed in numerical simulations (Turner et al. 1995; Burkert & Hartmann 2004; Hartmann & Burkert 2007; Vázquez-Semadeni et al. 2007; Heitsch et al. 2009; Rosas-Guevara et al. 2010; Prieto et al. 2011). Thus, the collapse of giant molecular clouds may proceed in a way that is anything but a monolithic, three-dimensional collapse.

5.2. Implications for the free-fall estimate of the SFR

A second implication of our results is that they may contribute, at least partially, towards alleviating the well known "star formation conundrum". The latter consists in that the observed star formation rate (SFR), of a few $M_\odot$ yr^{-1} (e.g., Smith et al. 1978; Diehl et al. 2006; Robitaille & Whitney 2010), is roughly two orders of magnitude lower than the simple estimate obtained by dividing the total molecular mass in the Galactic ISM

by the *three-dimensional* free-fall time corresponding to the mean density and temperature of the molecular gas (Zuckerman & Palmer 1974). This argument caused the dismiss of the original proposal by Goldreich & Kwan (1974) that molecular clouds should be in gravitational collapse, and was replaced by the notion that the observed linewidths correspond to supersonic microturbulence (Zuckerman & Evans 1974). The latter was thought to provide support against the clouds' self-gravity, a notion that persists until the present. Later on, support by magnetic fields was considered as well, and led to the notion that molecular clouds are in near virial equilibrium, with SF proceeding at a much slower rate than free-fall, only as allowed by mediation of ambipolar diffusion (see, e.g., the reviews by Shu et al. 1987; Mouschovias 1991) and of local turbulent compression (e.g., Vazquez-Semadeni et al. 2000; Mac Low & Klessen 2004).

However, if molecular clouds and their substructure are indeed in near free-fall, as suggested by various recent studies (e.g., Burkert & Hartmann 2004; Vázquez-Semadeni et al. 2007, 2010; Hartmann & Burkert 2007; Peretto, Hennebelle & André 2007; Galván-Madrid et al. 2009; Schneider et al. 2010; Csengeri et al. 2011a,b), then the SF conundrum reappears as a challenge to theoretical models of free-falling clouds (e.g., Zamora-Avilés & Vázquez-Semadeni 2011). Our results may imply that, if the cold (molecular and atomic) gas is distributed in sheets and filaments rather than in three-dimensional structures, as suggested by various observational studies (e.g., Bally et al. 1989; de Geus et al. 1990; Heiles & Troland 2003; Molinari et al. 2010; André et al. 2010), then the 3D value of the free-fall time is an underestimate to the real value, implying that the 3D free-fall SFR value overestimates its actual value, and that the severity of the SF conundrum may be reduced by up to one order of magnitude.

Of course, the correction provided by our results is not expected to provide a *full* solution to the SFR conundrum, since it is unlikely that sheets and filaments have the

required aspect ratio values of $A \sim$ a few $\times 10^3$ to completely account for a two-order-of-magnitude discrepancy between the observed and the free-fall estimate values of the SFR (see Figs. 1 and 2). Besides, the presence of even weak magnetic fields (implying supercritical mass-to-magnetic flux molecular clouds) and stellar feedback are expected to reduce the SFR beyond whatever is achieved by the possible low dimensionality of the clouds. Nevertheless, our result may provide a reduction of the discrepancy factor between the observed SFR and its free-fall estimate by factors ranging from a few to almost one order of magnitude, since observed aspect ratios of sheets and filaments in the ISM can reach values of up to 10^2 (Heiles & Troland 2003; Molinari et al. 2010).

6. Summary and Conclusions

We have computed the free fall time for two geometries that depart from spherical symmetry, namely, thin circular sheets and long filaments. In both cases, we considered two different behaviors for the volume density, one assuming that it remains constant through the collapse and the other assuming that it is the mass that remains constant, and the density increasing as the object collapses. These two cases should bracket the actual collapse timescale.

We have parameterized the problem by the aspect ratio A of the object, defined either as the ratio of the cloud's radius to its (small) thickness ($A = R/h$) in the case of sheets, or as the ratio of the cloud's half-length to its (small) radius ($A = L/\mathcal{R}$), in the case of filaments. Our calculations assume that the clouds contract only along their largest dimension (radially for sheets, and longitudinally for filaments), and thus our results are more accurate as larger values of A are considered. The value $A = 1$ is a frontier value between the two symmeties, although it is also the value for which our calculations are in largest error, since three-dimensional contraction should ensue in that case, with the

free-fall time being given by $\tau_{\rm ff,3D}$. Nevertheless, even in this extreme case, our calculations only deviate from the 3D value by factors of order unity.

For both cases, we found that the collapse time increases as $A^{1/2}$. In particular, this implies that the collapse time of a thin sheet is of the order of that of a sphere with much lower volume density, so that it is its *column* density that is the same as that of the sheet's. This result has two important implications for the structure of molecular clouds and star formation. First, it naturally explains the common morphology observed in molecular clouds, where star-forming or pre-stellar clumps are embedded within filaments that appear to be accreting onto them. According to our results, this is a natural consequence of the longer free-fall time for a filament than for any clump-like structure within it that contains enough mass to be itself collapsing. Because the filament has a longer collapse time, it will continue to accrete onto the locally collapsing 3D clump after the latter has managed to increase its density by a large enough amount as to become distinguishable from the filament.

Second, it may imply that, if molecular gas in the Galaxy is distributed in primarily low-dimensional structures such as sheets and filaments, then the so-called SFR conundrum may not be as strong as it is normally stated, because the relevant free-fall time for the cold gas in the Galaxy may be longer than has been considered. However, we expect that this effect is likely to only account for a fraction of the discrepancy between the observed and the free-fall prediction for the SFR, since the required aspect ratios to fully account for the conundrum would be too large ($A \sim$ a few $\times 10^3$), and besides other effects are known to contribute to reduce the SFR, such as magnetic fields and stelllar feedback. In any case, our results suggest that determining the topology of molecular clouds is important for estimating their true expected collapse timescales.

We acknowledge useful comments from an anonymous referee, which helped improving

the clarity and scope of the paper. This work has received financial support from grants CONACYT 102488 to E.V.-S., UNAM-DGAPA grant PAPIIT IN106511 to G.C.G, and a fellowship from CONACYT-SNI to J.A.T.

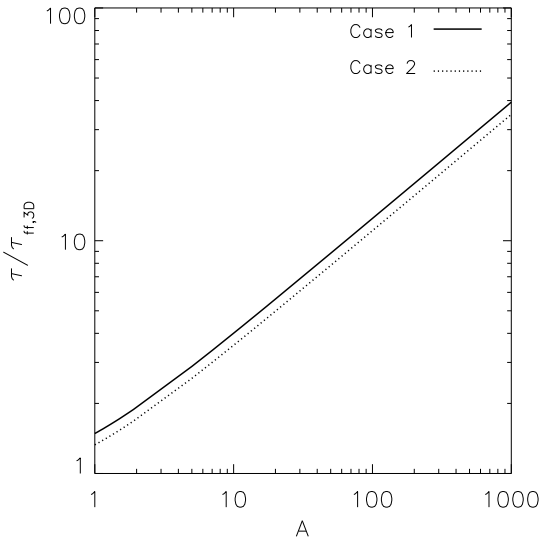

Fig. 3.— Dependence of the free-fall time for a filamentary cloud on the parameter A. The asymptotic behavior $\propto \sqrt{A}$ is seen to be reached quickly as A is increased.

REFERENCES

André, P., Men'shchikov, A., Bontemps, S., et al. 2010, A&A, 518, L102

Bally, J., Stark, A. A., Wilson, R. W., & Langer, W. D. 1989, The Physics and Chemistry of Interstellar Molecular Clouds - mm and Sub-mm Observations in Astrophysics, 331, 81

Binney, J., & Tremaine, S. 1987, Princeton, NJ, Princeton University Press, 1987,

Burkert, A., & Hartmann, L. 2004, ApJ, 616, 288

Csengeri, T., Bontemps, S., Schneider, N., Motte, F., & Dib, S. 2011, A&A, 527, A135

Csengeri, T., Bontemps, S., Schneider, N., et al. 2011, ApJ, 740, L5

Curry, C. L. 2000, ApJ, 541, 831

de Geus, E. J., Bronfman, L., & Thaddeus, P. 1990, A&A, 231, 137

Diehl, R., et al. 2006, Nature, 439, 45

Gaida, M., Ungerechts, H., & Winnewisser, G. 1984, A&A, 137, 17

Galván-Madrid, R., Keto, E., Zhang, Q., Kurtz, S., Rodríguez, L. F., & Ho, P. T. P. 2009, ApJ, 706, 1036

Goldreich, P. & Kwan, J. 1974, ApJ, 189, 441

Hanawa, T. et al. 1993, ApJ, 404 L83

Hartmann, L. & Burkert, A. 2004, ApJ, 616, 288

Heiles, C., & Troland, T. H. 2003, ApJ, 586, 1067

Heitsch, F., Hartmann, L. W., Slyz, A. D., Devriendt, J. E. G., & Burkert, A. 2008, ApJ, 674, 316

Heitsch, F., Ballesteros-Paredes, J., & Hartmann, L. 2009, ApJ, 704, 1735

Kofman, L., & Pogosyan, D. 1995, ApJ, 442, 30

Larson, R. B. 1985, MNRAS, 214, 379

Ledoux, P. 1951, Ann. d'Astrophys., 14, 438

Mac Low, M.-M., & Klessen, R. S. 2004, Reviews of Modern Physics, 76, 125

Molinari, S., Swinyard, B., Bally, J., et al. 2010, A&A, 518, L100

Mouschovias, T. C. 1991, NATO ASIC Proc. 342: The Physics of Star Formation and Early Stellar Evolution, 449

Myers, P. C. 2009, ApJ, 700, 1609

Peretto, N., Hennebelle, P., André, P. 2007, A&A, 464, 983

Pillai, T., Kauffmann, J., Wyrowski, F., et al. 2011, A&A, 530, A118

Pon, A., Johnstone, D., & Heitsch, F. 2011, arXiv:1108.1395

Prieto, J., Padoan, P., Jimenez, R., & Infante, L. 2011, ApJ, 731, L38

Purcell, C. R., Minier, V., Longmore, S. N., et al. 2009, A&A, 504, 139

Robitaille, T. P., & Whitney, B. A. 2010, ApJ, 710, L11

Rosas-Guevara, Y., Vázquez-Semadeni, E., Gómez, G. C., & Jappsen, A.-K. 2010, MNRAS, 406, 1875

Schneider, N., Csengeri, T., Bontemps, S., et al. 2010, A&A, 520, A49

Schneider, S., & Elmegreen, B. G. 1979, ApJS, 41, 87

Shu, F. H., Adams, F. C., & Lizano, S. 1987, ARA&A, 25, 23

Smith, L. F., Biermann, P., & Mezger, P. G. 1978, A&A, 66, 65

Tohline, J. E. 1980, ApJ, 239, 417

Turner, J. A., Chapman, S. J., Bhattal, A. S., et al. 1995, MNRAS, 277, 705

Vázquez-Semadeni, E., Colín, P., Gómez, G. C., Ballesteros-Paredes, J., Watson, A. W. 2010, ApJ, 715, 1302

Vázquez-Semadeni, E., Gómez, G. C., Jappsen, A. K., Ballesteros-Paredes, J., González, R. F., & Klessen, R. S. 2007, ApJ, 657, 870

Vazquez-Semadeni, E., Ostriker, E. C., Passot, T., Gammie, C. F., & Stone, J. M. 2000, Protostars and Planets IV, 3

Zamora-Avilés, M. A., & Vázquez-Semadeni, Enrique 2011, submitted to ApJ (arXiv:1105.4777)

Zuckerman B., & Evans N. J. 1974, ApJ, 192, L149

Zuckerman, B. & Palmer, P. 1974, ARA&A, 12, 279